

BVINet: Unlocking Blind Video Inpainting with Zero Annotations

Zhiliang Wu, Kerui Chen, Kun Li, Hehe Fan, Yi Yang

ReLER Lab, CCAI, Zhejiang University

Abstract

Video inpainting aims to fill in corrupted regions of the video with plausible contents. Existing methods generally assume that the locations of corrupted regions are known, focusing primarily on the “how to inpaint”. This reliance necessitates manual annotation of the corrupted regions using binary masks to indicate “where to inpaint”. However, the annotation of these masks is labor-intensive and expensive, limiting the practicality of current methods. In this paper, we expect to relax this assumption by defining a new blind video inpainting setting, enabling the networks to learn the mapping from corrupted video to inpainted result directly, eliminating the need of corrupted region annotations. Specifically, we propose an end-to-end blind video inpainting network (BVINet) to address both “where to inpaint” and “how to inpaint” simultaneously. On the one hand, BVINet can predict the masks of corrupted regions by detecting semantic-discontinuous regions of the frame and utilizing temporal consistency prior of the video. On the other hand, the predicted masks are incorporated into the BVINet, allowing it to capture valid context information from uncorrupted regions to fill in corrupted ones. Besides, we introduce a consistency loss to regularize the training parameters of BVINet. In this way, mask prediction and video completion mutually constrain each other, thereby maximizing the overall performance of the trained model. Furthermore, we customize a dataset consisting of synthetic corrupted videos, real-world corrupted videos, and their corresponding completed videos. This dataset serves as a valuable resource for advancing blind video inpainting research. Extensive experimental results demonstrate the effectiveness and superiority of our method.

1. Introduction

Video inpainting is a fundamental visual restoration task in computer vision, aiming to fill corrupted regions in videos with plausible and coherent contents [44–46]. Existing video inpainting methods [2, 7, 28, 34, 46, 51, 52, 54, 58] typically take corrupted videos along with masks indicating

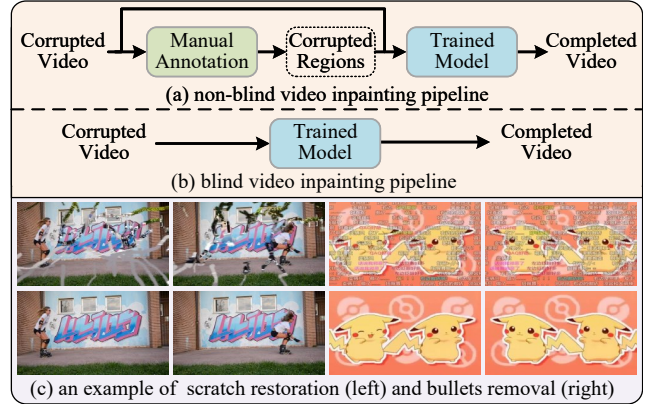


Figure 1. Fig.(a) shows the general pipeline of existing non-blind video inpainting. Such pipeline require manual annotation of corrupted regions of each frame, limiting its application scope. In this paper, we formulate a new task: blind video inpainting, which can directly learn a mapping from corrupted video to inpainted result without any corrupted region annotation (Fig.(b)). Fig.(c) shows an example of our blind video inpainting method in scratch restoration and bullet removal.

corrupted regions as input, and generate corrupted contents based on spatial texture and temporal information of valid (uncorrupted) regions. This means that these methods require manual annotation of corrupted regions using binary masks to indicate “where to inpaint”. We refer to this case as a *non-blind setting*. Nevertheless, accurate mask annotations are not available in many scenarios. On the one hand, the boundary between corrupted regions and valid regions is often blurred, making it unrealistic to accurately annotate corrupted regions. On the other hand, manual annotation is labor-intensive and resource-consuming, especially for corrupted videos with high frame rates and high resolutions.

In this paper, we formulate a novel task: *blind video inpainting*, where a mapping from corrupted videos to inpainted results is directly learned without any corrupted region annotation. Unlike the non-blind setting, which only focuses on “how to inpaint”, our proposed blind video inpainting setting requires considering both “where to inpaint” and “how to inpaint” simultaneously. This blind video inpainting setting is more effective in real-world ap-

plications. In fact, the “corruption” faced by video inpainting can be divided into two types. The first type of “corruption” is not present in the original video. This type of “corruption” is caused by external factors and destroys the original structure of the video, such as scratches [5, 47], watermarks [45, 56], and bullets [16], etc. Another type of “corruption” exists in the original video itself, such as undesired objects and occlusions [36, 40]. In this paper, we mainly focus on the first type of “corruption”.

For blind video inpainting task, a naive solution is to process corrupted video frame by frame using existing blind image inpainting methods [35, 39, 42]. However, such a solution will neglect the motion continuity between frames, resulting in flicker artifacts in the completed video. In this paper, we propose an end-to-end blind video inpainting framework consisting of a mask prediction network and a video completion network. The former aims to estimate the corrupted regions that need to be completed, while the latter focuses on completing the corrupted video. Specifically, we first develop a mask prediction network to predict the corrupted regions of whole video by detecting semantic-discontinuous regions of the frame and utilizing temporal consistency prior of the video. Then, we design a video completion network to perceive valid context information from uncorrupted regions using predicted mask to generate corrupted contents. To precisely capture the accurate correspondence between the mask prediction network and video completion network, we introduce a consistency loss to regularize their parameters, enabling mutual constraint and maximizing the overall model performance.

Furthermore, existing video inpainting datasets [5, 14, 19, 52] usually introduce specific prior knowledge during the construction process, such as corrupted content, clear border, and fixed shape. These priors make corrupted regions easily distinguishable from natural video frame by the mask prediction network, failing to realistically simulate the complex real-world scenarios in blind video inpainting. In this paper, we exploit free-form strokes [5] as corrupted regions, and fill these regions with natural images as corrupted contents. Such operations allow us to construct the corrupted contents with variable shapes, complex motions and faithful texture. To avoid the introducing border priors, we also utilize iterative Gaussian smoothing [41] to extend the edges of corrupted regions, making these boundaries difficult to distinguish. Such strategy can enforce the network to infer the corrupted regions by the semantic context of the video frame rather than merely fitting to the training data. Further, to enhance the generalization ability of our model in practical applications, we collect a bullet removal dataset consisting of 1,250 video clips. Extensive experimental results demonstrate that our method can achieve comparable performance to non-blind baselines. An example result of our method in scratch restoration and bullets

removal is shown in Fig.1(c).

To sum up, our contributions are summarized as follows:

- A novel blind video inpainting task is formulated. It directly learns a mapping from corrupted videos to inpainted results without any corrupted region annotation. To the best of our knowledge, this is the first blind inpainting work in the field of video inpainting.
- An end-to-end blind video inpainting framework consisting of a mask prediction network and a video completion network is designed, and a consistency loss is introduced to regularize the training parameters of this framework.
- A dataset suitable for blind video inpainting task is customized. This dataset consists of 2,400 synthesized video clips and 1,250 real-world video clips, and will be published to facilitate subsequent research.

2. Related Works

Non-Blind Video Inpainting. The video inpainting methods can be roughly divided into three lines: 3D convolution-based [5, 16, 29], flow-based [9, 14, 15, 26, 50, 53, 61], and attention-based methods [2, 19, 20, 28, 34, 36, 38, 52, 54].

The methods [5, 16, 29] based on 3D convolution usually reconstruct the corrupted contents by directly aggregating complementary information in a local temporal window through 3D temporal convolution. Nevertheless, they often yield temporally inconsistent completed results due to the limited temporal receptive fields. The methods [9, 14, 15, 26, 50, 53, 61] based on optical flow treat the video inpainting as a pixel propagation problem. Generally, they first introduce a deep flow completion network to complete the optical flow, and then utilize the completed flow to guide the valid pixels into the corrupted regions. However, these methods fail to capture the visible contents of long-distance frames, thus reducing the inpainting performance in the scene of large objects and slowly moving objects.

Due to its outstanding long-range modeling capacity, attention-based methods, especially transformer-based methods, have shed light on the video inpainting community. These methods [2, 19, 20, 28, 34, 36, 38, 52, 54] first find the most relevant pixels in the video frame with the corrupted regions by the attention module, and then aggregate them to complete the video frame. Although the existing video inpainting methods have shown promising results, they usually need to elaborately annotate the corrupted regions of each frame in the video, limiting its application scope. Unlike these approaches, we propose a blind video inpainting network in this paper, which can automatically identify and complete the corrupted regions in the video.

Blind Image Inpainting. In contrast to video inpainting, image inpainting solely requires consideration of the spatial consistency of the inpainted results. In the few years, the success of deep learning has brought new opportunities to many vision tasks, which promoted the development

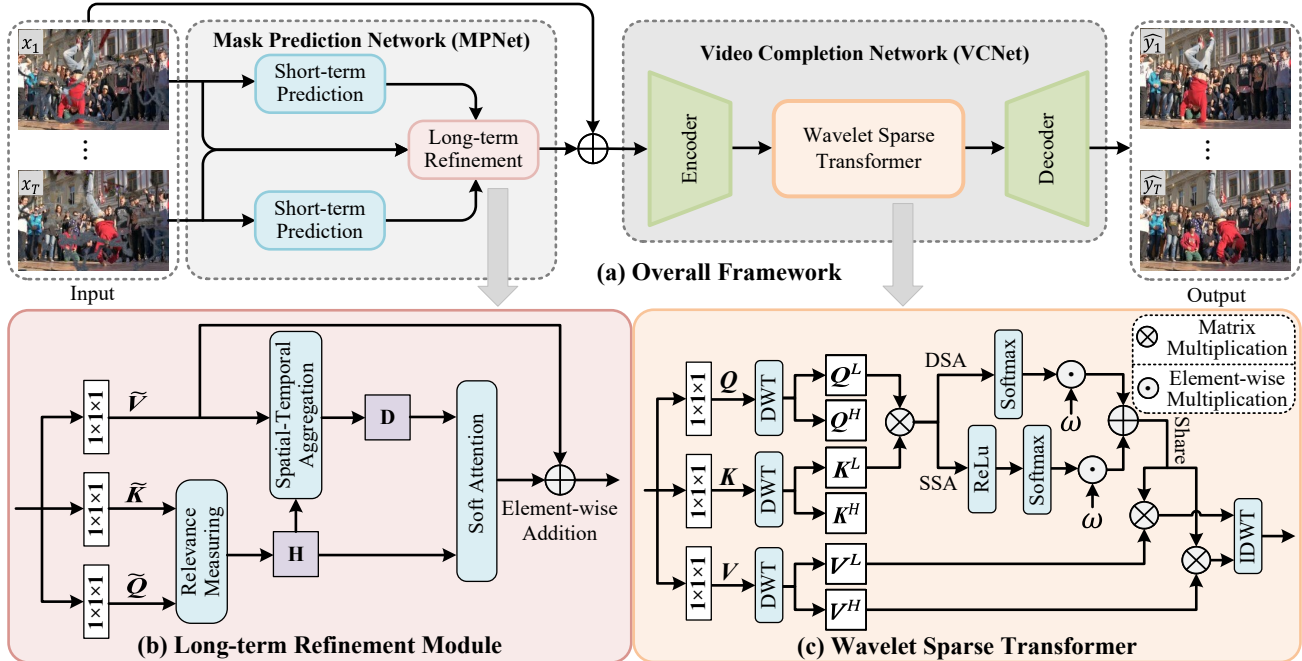


Figure 2. **The overview of the proposed blind video inpainting framework.** Our framework are composed of a mask prediction network (MPNet) and a video completion network (VCNet). The former aims to predict the masks of corrupted regions by detecting semantic-discontinuous regions of the frame and utilizing temporal consistency prior of the video, while the latter perceive valid context information from uncorrupted regions using predicted mask to generate corrupted contents.

of a large number of deep learning-based image inpainting methods [4, 8, 24, 27, 37]. As a sub-task of image inpainting, blind image inpainting [21, 25, 39, 42, 57] has been preliminarily explored. For example, Nian et al. [3] proposed a novel blind inpainting method based on a fully convolutional neural network. Liu et al. [30] designed a deep CNN to directly restore a clear image from a corrupted input. However, these blind inpainting work assumes that the corrupted regions are filled with constant values or Gaussian noise, which may be problematic when corrupted regions contain unknown content. To improve the applicability, Wang et al. [42] relaxed this assumption and proposed a two-stage visual consistency network. Compared with blind image inpainting, blind video inpainting presents an additional challenge in preserving temporal consistency. Naively applying blind image inpainting algorithms on individual video frame to fill corrupted regions will lose inter-frame motion continuity, resulting in flicker artifacts. Inspired by the success of deep learning in blind image inpainting task, we propose the first deep blind video inpainting model in this paper, which provides a strong benchmark for subsequent research.

3. Proposed Method

3.1. Problem Formulation

Given a corrupted video sequence $X = \{x_1, x_2, \dots, x_T\}$ with sequence length T . The corrupted regions of video se-

quence X are denoted as a binary mask $M = \{m_1, m_2, \dots, m_T\}$. For each mask m_i , “0” indicates that corresponding pixel is corrupted, and “1” denotes the valid regions. The goal of video inpainting is to generate a complete video sequence $\hat{Y} = \{\hat{y}_1, \hat{y}_2, \dots, \hat{y}_T\}$, which should be spatially and temporally consistent with the ground truth $Y = \{y_1, y_2, \dots, y_T\}$. Formally, existing video inpainting methods [2, 28, 34, 52, 54] aim to model the conditional distribution $p(\hat{Y}|X, M)$ by training a deep neural network \mathcal{D} , i.e., $\hat{Y} = \mathcal{D}(X, M)$. Nevertheless, these methods are only applicable when the corrupted region mask m_i of each video frame x_i is available. In practice, accurate mask of corrupted regions is difficult to manually annotate due to the blurred boundary between the corrupted regions and the valid regions. Furthermore, collecting these manual annotation mask is not only labor-intensive and time-consuming, but also often subjective and error-prone.

Different from existing video inpainting [2, 28, 34, 52, 54], we focus on video inpainting without any manual annotation mask of corrupted regions, called **blind video inpainting**. This task aims to learning a direct mapping \mathcal{G} from the corrupted video X to the completed video \hat{Y} i.e., $\hat{Y} = \mathcal{G}(X)$. It means that the mapping \mathcal{G} needs not only to automatically locate the corrupted regions, but also complete them. Towards this end, we decompose the blind video inpainting task into two sub-tasks: *mask prediction* and *video completion*. The former aims to estimate the corrupted regions of video, indicating “where to inpaint”, while the latter focus

to complete the corrupted regions of video, addressing “how to inpaint”. The dual sub-tasks are defined as follows:

- **mask prediction:** given a corrupted video sequence X , it learns the mapping Φ to predict the corrupted region masks M , *i.e.*, $M = \Phi(X)$;
- **video completion:** based on the predicted region masks M , it learns the mapping Ψ to generate the completed video sequence \hat{Y} , *i.e.*, $\hat{Y} = \Psi(X, M)$.

3.2. Network Design

In this paper, we design an end-to-end trainable framework to tackle blind video inpainting task. As shown in Fig.2(a), our framework consists of a mask prediction network and a video completion network. The former aims to predict the corrupted regions of entire video by detecting semantic-discontinuous regions of the frame and utilizing temporal consistency prior of the video, while the latter perceive valid context information from uncorrupted regions using predicted masks to generate corrupted contents.

3.2.1. Mask Prediction Network

As shown in Fig.2(a), our mask prediction network sub-network consists of a short-term prediction module and a long-term refinement module. The short-term prediction module takes the individual video frame x_i as input to predict the binary mask m_i^s of visual inconsistency regions, thus providing initial input for the long-term refinement module. The long-term refinement module is used to refine T predicted masks $M^s = \{m_1^s, m_2^s, \dots, m_T^s\}$ using the temporal consistency priors of videos.

Short-Term Prediction Module. The short-term prediction module is designed as an encoder-decoder structure. Specifically, the encoder consists of three stages, which generate feature maps at three different scales. All stages share a similar structure, which consists of multiple convolutional layers and residual blocks with ReLU activation functions. In contrast, the decoder is used to decode the learned features into the binary masks, and its architecture is similar to that of the encoder. Furthermore, researchers have demonstrated that noise can significantly reduce image segmentation performance [22, 23]. To enhance the noise immunity of CNN, Li et al. [22, 23] replaced the max-pooling, strided-convolution, and average-pooling in CNN with DWT, thereby achieving higher image segmentation accuracy. Motivated by such observation, we employ DWT to perform the down-sampling operation in the short-term prediction module. In this way, the short-term prediction module can obtain a more accurate mask of corrupted regions. Formally, the entire mask prediction process can be expressed as:

$$m_i^s = STP(x_i), \quad (1)$$

where STP denotes short-term prediction module. m_i^s is the predicted mask of the i -th video frame x_i .

Long-Term Refinement Module. The long-term refinement module consists of three main parts: encoder, sequence-to-sequence transformer, and decoder, where the encoder and decoder have the same backbone as the encoder and decoder of the short-term refinement module. Sequence-to-sequence transformer is the core component of the long-term refinement module. It aims to refine $M^s = \{m_1^s, m_2^s, \dots, m_T^s\}$ using the temporal consistency priors.

As shown in Fig.2(b), for deep features $E = \{e_1, e_2, \dots, e_T\}$ extracted with encoder through cascading the corrupted video sequence X and mask M^s , we first project them into query (Q), key (K) and value (V) using a $1 \times 1 \times 1$ convolutional layer. After obtaining Q , K , and V , they are split into N groups $\{\tilde{Q}_n, \tilde{K}_n, \tilde{V}_n\} \in \mathbb{R}^{T \times H \times W \times \frac{C}{N}}$ along the channel dimension, where $n \in \{1, 2, \dots, N\}$.

Then, we measure the relevance between \tilde{Q}_n and \tilde{K}_n to extract the spatial-temporal relationship between video frames. However, the positions of corrupted regions in adjacent frames are similar [10, 13]. Therefore, we use the surrounding neighborhood obtained from a response window to compute a spatial-temporal affinity matrix H_n of the target pixel, instead of computing the response between a query position and the features at all positions. Such a relevance measurement captures more relevance related to the target regions within T frames.

Having the affinity matrix H_i , we calculate the spatial-temporally aggregated features D_n within the surrounding neighborhood by matrix multiplication between the response window of \tilde{V}_n and the affinity matrix H_n . Finally, a soft-attention block is used to synthesize features from the group of affinity matrix H_i and aggregated features D_i . During the synthesis process, relevant spatial-temporal patterns should be enhanced while less relevant ones should be suppressed. To achieve that, a soft-attention map G is generated by taking the channel-wise maximum value on H , which is obtained by concatenating a group of the affinity matrix H_i along the channel dimension. In summary, the synthesized features \hat{E} are calculated as follows:

$$\hat{E} = E + Conv(D) \odot G, \quad (2)$$

where $Conv$ and \odot represent the convolutional and element-wise multiplication operation, respectively. D is obtained by concatenating a group of the spatial-temporally aggregated features D_i along the channel dimension.

3.2.2. Video Completion Network

Video completion network aims to perceive valid context information from uncorrupted regions using predicted mask to generate corrupted contents, which is in line with the goal of video inpainting task in non-blind settings. Recently, benefiting from the advantages of long-range feature capture capacity, transformer-based video inpainting methods [2, 28, 34, 52, 54] have achieved unprecedented performance in non-blind settings. These methods typically

retrieve relevant contents to fill the corrupted regions by a self-attention mechanism. However, they still suffer from two major limitations. Firstly, these methods always aggregate the features using all attention relations based on query-key pairs to generate the corrupted contents. Such an aggregation will lead to the redundant or irrelevant contents being filled into the corrupted regions, causing blurry or compromised results [6, 60]. Secondly, these methods typically utilize the whole features to calculate self-attention. Such a setting ignores the impact of noise in the features on attention calculation, significantly reducing the accuracy of attention retrieval [48]. Based on this, we design a wavelet sparse transformer as our video completion network to generate corrupted contents.

As shown in Fig.2(c), for the features $F = \{f_1, f_2, \dots, f_T\}$ extracted by encoder, we first map each $f_i \in \mathbb{R}^{h \times w \times c}$ into query (Q_i), key (K_i), and value (V_i) to establish deep correspondences for each region in different semantic spaces. Having Q_i , K_i , and V_i , we decompose them into different frequencies by Discrete Wavelet Transform (DWT) [31]. Such a strategy can isolate the noise into the high-frequency components $Q_i^H, K_i^H, V_i^H \in \mathbb{R}^{3 \times \frac{h}{2} \times \frac{w}{2} \times c}$, allowing the low-frequency components $Q_i^L, K_i^L, V_i^L \in \mathbb{R}^{\frac{h}{2} \times \frac{w}{2} \times c}$ only contain relatively clean basic features.

After obtaining all low-frequency components, we use them to calculate standard dense self-attention (DSA):

$$DSA = \text{Softmax} \left(\frac{Q^L \cdot (K^L)^T}{\sqrt{d}} + B \right), \quad (3)$$

where *Softmax* denotes the softmax layer. B refers to the learnable relative positional bias. Since not all query tokens are closely relevant to corresponding ones in keys, the utilization of all similarities is ineffective for generation corrupted contents. Instead, it leads to the redundant or irrelevant contents being filled into the corrupted regions, causing blurry or compromised results.

Intuitively, developing a sparse self-attention (SSA) mechanism to aggregate the most relevant features could improve inpainting performance. Inspired by adaptive sparse self-attention [60], we utilize ReLU to remove negative similarities, preserving the most significant contents:

$$SSA = \text{Softmax} \left(\text{ReLU} \left(\frac{Q^L \cdot (K^L)^T}{\sqrt{d}} \right) + B \right), \quad (4)$$

where *ReLU* denotes the ReLU layer. Note that simply using *SSA* will impose over sparsity, making the learned feature representation insufficient to produce the complete corrupted contents. Conversely, using *DSA* will inadvertently introduce irrelevant features into corrupted regions, leading to blurry results. Therefore, we design a two-branch self-attention mechanism to calculate attention, maximizing the

advantages of both two paradigms. The completed features of different frequencies can be obtained by a shared attention manner:

$$\begin{aligned} \widehat{V}^L &= (\omega_1 \odot DSA + \omega_2 \odot SSA) V^L, \\ \widehat{V}^H &= (\omega_1 \odot DSA + \omega_2 \odot SSA) V^H, \end{aligned} \quad (5)$$

where ω_1 and ω_2 are two normalized weights for adaptively modulating two-branch. \widehat{V}^L and \widehat{V}^H denote the completed low-frequency components and completed high-frequency components, respectively. In this way, the negative impact of noise on attention calculation can be significantly mitigated, thereby achieving the goal of improving the inpainting performance. Finally, we utilize Inverse Discrete Wavelet Transform (IDWT) to obtain the final completed features \widehat{V} . Note that we only borrow information from valid regions to generate corrupted contents. Therefore, we set the *DSA* and *SSA* in corrupted regions to 0.

3.3. Consistency Constraints

In our framework, mask prediction network and video completion network are closely correlated and mutually constrained. The former helps the latter to locate the corrupted regions, while the latter regularizes the former by the reconstruction loss, enforcing it to focus on corrupted regions.

Ideally, if mask prediction network and video completion network both can capture accurate correspondence, the difference between the corrupted video frame x_i and the completed result \widehat{y}_i should exist only in the corrupted regions. This means that the following relationship holds:

$$m_i = \mathcal{B}(\widehat{y}_i - x_i), \quad (6)$$

$$m_i^l = \mathcal{B}(\widehat{y}_i - x_i), \quad (7)$$

where \mathcal{B} denotes binarization operation. m_i^l and m_i are the mask obtained by mask prediction network and ground truth mask, respectively.

Eq.(6) and Eq.(7) give us the solution to further constraint mask prediction network and video completion network by a consistency loss. The consistency loss \mathcal{L}_c is formulated as follows:

$$\mathcal{L}_c = \|m_i^l - \mathcal{B}(\widehat{y}_i - x_i)\|_1 + \|m_i - \mathcal{B}(\widehat{y}_i - x_i)\|_1. \quad (8)$$

3.4. Loss Functions

We train our network by minimizing the following loss:

$$\mathcal{L} = \lambda_m \mathcal{L}_m + \lambda_v \mathcal{L}_v + \lambda_c \mathcal{L}_c, \quad (9)$$

where \mathcal{L}_m , \mathcal{L}_v , and \mathcal{L}_c denote mask prediction loss, video completion loss and consistency loss, respectively. λ_m , λ_v and λ_c are non-negative trade-off parameters. In our experiments, λ_m , λ_v and λ_c are set to 3, 5 and 0.02, determined by grid searching. More details of our framework and loss function can be found in the [supplementary materials](#).

Table 1. Quantitative results of video inpainting on YouTube-VOS and DAVIS datasets. The term *Blind* denotes ‘Blind setting’ for short.

Methods	Blind	YouTube-VOS				DAVIS			
		PSNR↑	SSIM↑	E_{warp} ↓	LPIPS↓	PSNR↑	SSIM↑	E_{warp} ↓	LPIPS↓
TCCDS [12]	✗	23.418	0.8119	0.3388	1.9372	28.146	0.8826	0.2409	1.0079
VINet [16, 17]	✗	26.174	0.8502	0.1694	1.0706	29.149	0.8965	0.1846	0.7262
DFVI [50]	✗	28.672	0.8706	0.1479	0.6285	30.448	0.8961	0.1640	0.6857
FGVC [9]	✗	24.244	0.8114	0.2484	1.5884	28.936	0.8852	0.2122	0.9598
CPVINet [19]	✗	28.534	0.8798	0.1613	0.8126	30.234	0.8997	0.1892	0.6560
STTN [52]	✗	28.993	0.8761	0.1523	0.6965	28.891	0.8719	0.1844	0.8683
FuseFormer [28]	✗	29.765	0.8876	0.1463	0.5481	29.627	0.8852	0.1767	0.6706
E2FGVI [26]	✗	30.064	0.9004	0.1490	0.5321	31.941	0.9188	0.1579	0.6344
FGT [54]	✗	30.811	0.9258	0.1308	0.4565	32.742	0.9272	0.1669	0.4240
ProPainter [59]	✗	29.906	0.9050	0.1458	0.4962	31.967	0.9250	0.1655	0.4370
WaveFormer [48]	✗	33.264	0.9435	0.1184	0.2933	34.169	0.9475	0.1504	0.3137
VCNet (Ours)	✗	34.107	0.9521	0.1102	0.2145	34.936	0.9561	0.1362	0.2706
MPNet+CPVINet	✓	25.206	0.8115	0.2045	1.2269	26.024	0.8296	0.2178	1.2543
MPNet+STTN	✓	25.049	0.8295	0.2032	1.6490	25.009	0.8505	0.2882	1.4868
MPNet+FuseFormer	✓	25.269	0.8302	0.2062	1.6772	24.752	0.8260	0.2887	1.4351
MPNet+E2FGVI	✓	26.422	0.8368	0.1832	1.1145	27.318	0.8536	0.1871	0.9523
MPNet+FGT	✓	27.032	0.8755	0.1609	0.8667	28.387	0.8963	0.1759	0.7392
MPNet+WaveFormer	✓	29.185	0.8902	0.1508	0.7153	29.794	0.9016	0.1607	0.7669
Ours	✓	30.528	0.9088	0.1362	0.6556	30.961	0.9107	0.1565	0.7338

4. Experiments

4.1. Dataset Customization

Training Dataset. Existing datasets [5, 14, 19, 52] usually generate corrupted video by $\mathbf{x}_i = (1 - \mathbf{m}_i) \odot \mathbf{y}_i + \mathbf{m}_i \odot \mathbf{u}_i$, where \mathbf{u}_i is a pre-defined noise, \odot is the element-wise multiplication operation. The non-blind setting always assume that the noise \mathbf{u}_i is the “0” pixel value. In this scenario, the corrupted regions \mathbf{m}_i in corrupted video frame \mathbf{x}_i can be easily identified and predicted by the prior knowledge introduced in the dataset, such as corrupted contents, clear border, and fixed shape. Therefore, these datasets fail to realistically simulate the complex real-world scenarios in blind video inpainting.

In this paper, we customize a dataset suitable for blind video inpainting task. Specifically, we first utilize free-form strokes [5] as our corrupted regions \mathbf{m}_i , and fill \mathbf{m}_i with real-world image patches as corrupted contents \mathbf{u}_i . In this way, the generated corrupted contents have variable shapes, complex motions and faithful texture, effectively avoiding the introduction of shape and contents prior in the dataset.

After obtaining the corrupted regions \mathbf{m}_i and corrupted contents \mathbf{u}_i , the corrupted video frame \mathbf{x}_i can be generated by $\mathbf{x}_i = (1 - \mathbf{m}_i) \odot \mathbf{y}_i + \mathbf{m}_i \odot \mathbf{u}_i$. However, the corrupted frame \mathbf{x}_i obtained in this way often results in noticeable edges, which can serve as a strong indicator for identifying corrupted regions. It may inadvertently encourage the model to learn and rely on this prior knowledge, ultimately compromising its ability to understand the semantic content

of the video. To avoiding the introduction of obvious edge priors, an iterative Gaussian smoothing [41] is introduced to extend the contact regions between \mathbf{u}_i and \mathbf{y}_i . Such strategy can enforce the network to infer the corrupted regions by the semantic context of the video frame, rather than merely fitting to the training data.

Finally, to enhance the generalization ability of the model in practical applications, we also collect 1,250 bullet removal video clips. We customized dataset consists of 2,400 synthesized video clips and 1,250 real-world video clips for blind video inpainting tasks. This dataset will be published to facilitate subsequent research.

Testing Dataset. To verify the effectiveness of the proposed blind video inpainting method, we employ two widely used datasets, namely Youtube-vos [49] and DAVIS [32], for evaluation. Following the previous works [20, 50], 508 and 60 video clips of the Youtube-vos and the DAVIS are used as test sets to calculate metrics, respectively. Meanwhile, the corrupted contents of these test sets are synthesized using a similar manner to the training set.

4.2. Baselines and Metrics

To the best of our knowledge, there is no work focusing on deep blind video inpainting task. Therefore, we use sixteen methods as our baselines to evaluate the blind video inpainting ability of our model, including eleven non-blind video inpainting methods, *i.e.*, TCCDS [12], VINet [16, 17], DFVI [50], CPVINet [19], FGVC [9], STTN [52], FuseFormer [28], E2FGVI [26], FGT [54], ProPainter [59], and WaveFormer [48], and six blind video inpainting

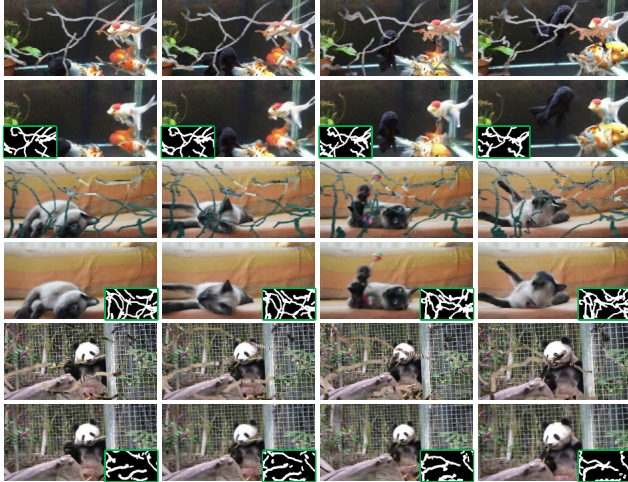


Figure 3. Three example of inpainting results with our method. The top row shows corrupted video frame. The completed results are shown in the bottom row, where green box denotes the mask generated by the model.

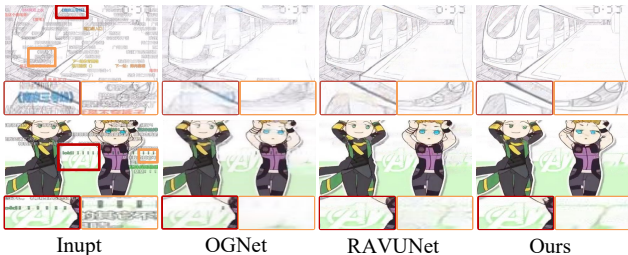


Figure 4. Qualitative results compared with OGNet [33] and RAVUNet [1] on bullet removal.

methods, *i.e.*, MPNet+CPVINet [19], MPNet+STTN [52], MPNet+FuseFormer [28], MPNet+E2FGVI [26], MPNet+FGT [54], and MPNet+WaveFormer [48]. To ensure the fairness of the experimental results, non-blind video inpainting baselines follow their original non-blind settings (including model input and test datasets), while blind video inpainting baselines are fine-tuned on our synthesized dataset using their released models and codes. Similar to the previous works [43, 45], we employ four metrics to report quantitative results, *i.e.*, PSNR [11], SSIM [36], LPIPS [55] and flow warping error E_{warp} [18].

4.3. Experimental Results on Synthesized Dataset

We report the quantitative evaluation results of our method and other baselines in Tab. 1. As shown in this table, the PSNR, SSIM, E_{warp} and LPIPS of our method achieve state-of-the-art results under blind inpainting settings on two datasets, and have obtained comparable performance with non-blind video inpainting methods. In particular, for blind inpainting settings, our method outperforms the best baseline (MPNet+FGT [54]) with a large margin in all

Table 2. Ablation study of MPNet.

Methods	BCE↓	IOU↑	Methods	BCE↓	IOU↑
STP	1.1251	0.8437	DWT_STP	1.0785	0.8682
DWT_STP+LTR	0.9176	0.8829	Full MPNet	0.8052	0.9017

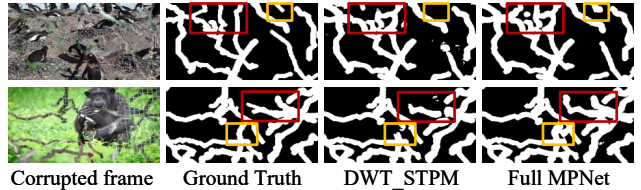


Figure 5. Example of corrupted regions segmentation.

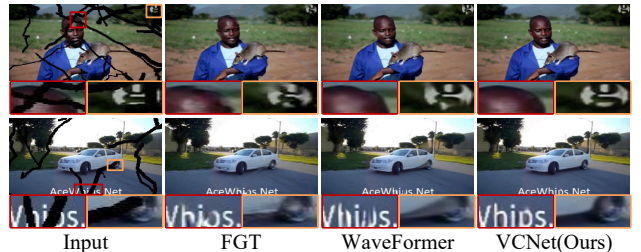


Figure 6. Comparison of qualitative results under non-blind settings. Better viewed at zoom level 400%.

evaluation metrics. Compared with video inpainting methods under non-blind settings, our blind inpainting model achieves a comparable performance to the sub-optimal baseline E2FGVI [26]. This verifies the superiority and effectiveness of the proposed blind video inpainting approach. To further compare the visual qualities of inpainted results, we show the inpainted results for our model on three examples in Fig. 3. As can be observed, our method can obtain spatial-temporally consistent inpainted results without any mask annotations. This demonstrates the effectiveness of the proposed method. More blind video inpainting results can be found in the [supplementary materials](#).

4.4. Experimental Results on Real Cases

The proposed blind video inpainting method is beneficial for many practical applications, such as bullet removal. Fig. 4 compares the results of bullet removal between OGNet [33], RAVUNet [1], and our method. As shown in Fig. 4, our method effectively eliminates bullets in videos without the need for any mask annotations, and generates better details than the baselines. This results further demonstrate the effectiveness and superiority of our method in practical applications. More real cases can be found in the [supplementary materials](#).

4.5. Ablation Studies

Effectiveness of MPNet. We conduct an ablation study on the proposed MPNet. As shown in Tab. 2, we compare the full MPNet model with its three variants, *i.e.*, “STPM”,



Figure 7. (a) Visual evaluations with random masks filled with different content (first four examples). (b) Visual comparison of different masks filled with the same content (last four examples). Better viewed at zoom level 400%.

Table 3. Ablation study of sparse self-attention and \mathcal{L}_c .

DSA	SSA	\mathcal{L}_c	PSNR \uparrow	SSIM \uparrow	E_{warp} \downarrow	LPIPS \downarrow
✓			29.172	0.8897	0.1529	0.7264
✓	✓		29.885	0.8962	0.1454	0.6891
✓	✓	✓	30.528	0.9088	0.1362	0.6556

“DWT_STPM”, and “DWT_STPM+LTRM”. First two variants refer to down-sampling in the short-term prediction module using the strided-convolution and the DWT, separately. The third variant refines the prediction result of the second variant using strided-convolution for down-sampling in the long-term refinement module. The results indicate that the full MPNet model achieves the best prediction performance of corrupted regions, with the values of 0.8052 and 0.9017 for binary cross entropy (BCE) and intersection over union (IOU), respectively. Besides, we also show the predicted results of the full MPNet model and the second variant. As revealed in Fig. 5, the corrupted regions predicted by the full MPNet model are closer to ground-truth. This demonstrates that the effectiveness of MPNet.

Effectiveness of VCNet. To demonstrate the effectiveness of VCNet, we compare it with ten non-blind video inpainting methods. As shown in Tab. 1, our VCNet achieves substantial improvements on all four quantitative metrics. Furthermore, we also display some qualitative comparisons with two representative methods, including FGT [54] and WaveFormer [48]. As shown in Fig. 6, our VCNet can generate faithful texture and structure information, which verifies the effectiveness and superiority of VCNet.

Effectiveness of Sparse Self-Attention. In Tab. 3, we perform an ablation study for sparse self-attention. From the table, we can observe that: 1) The model using only the dense self-attention (DSA) branch achieves the worst inpainting performance due to the introduction of irrelevant features. 2) Using sparse self-attention (SSA) branches improves the inpainted performance of the model. These results further demonstrates the necessity of an adaptive selection strategy for video inpainting task.

Effectiveness of Consistency Loss \mathcal{L}_c . \mathcal{L}_c is introduced to regularize the training parameters, enforcing mask prediction network and video completion network to capture accurate correspondence. Tab. 3 presents an ablation study on \mathcal{L}_c . As shown in Tab. 3, the models with \mathcal{L}_c participating in training can obtain better inpainted results.

Robustness against Various Degradation Patterns. In

Table 4. Efficiency analysis.

Metrics	STTN [52]	FuseFormer [28]	E2FGVI [26]	FGT [54]	VCNet(Ours)
FLOPs	477.91G	579.82G	442.18G	455.91G	396.35G
Time	0.22s	0.30s	0.26s	0.39s	0.21s

Fig. 7(a), we filled the corrupted regions of the video with different contents to perform the inpainting experiment. As shown in figure, our model can handle Gaussian noise or constant color fills, even though these patterns are not included in the training dataset. These results suggest that our model can learn to identify and inpaint the visually inconsistent regions in video frames, rather than simply memorizing the data distribution of the synthetic dataset.

Robustness against Various Corrupted Patterns. We conduct an ablation study for corrupted patterns. As illustrated in Fig. 7(b), our blind video inpainting model can effectively handle corrupted regions of various patterns, and generates visually pleasing results. This indicates that our method is highly robust to the patterns of corrupted regions.

Efficiency Analysis. We compare the efficiency of our VCNet with STTN [52], FuseFormer [28], E2FGVI [26] and FGT [54] on two metrics: FLOPs and inference time. Following previous works [28, 52, 54], we measure FLOPs with a temporal size (number of frames) of 20. The inference time is measured on a single Titan RTX. As shown in Tab. 4, our VCNet achieves the fastest inference speed and lowest FLOPs compared to baselines. This also further indicates that our full model (MPNet+VCNet) is more efficient than MPNet+STTN [52], MPNet+FuseFormer [28], MPNet+E2FGVI [26], and MPNet+FGT [54].

5. Conclusion

In this paper, we formulate a novel blind video inpainting task, which aims to achieve video inpainting without any corrupted regions annotation. For this purpose, we design an end-to-end blind video inpainting framework consisting of a mask prediction network and a video completion network, and a consistency loss is introduced to regularize the training parameters. Furthermore, we customize a dataset suitable for blind video inpainting, which can effectively facilitate subsequent researches. Experimental results demonstrate the effectiveness of the our method.

References

- [1] Lorenzo Agnolucci, Leonardo Galteri, Marco Bertini, and Alberto Del Bimbo. Restoration of analog videos using swin-unet. In *Proceedings of the 30th ACM International Conference on Multimedia (ACMMM)*, pages 6985–6987, 2022. 7
- [2] Jiayin Cai, Changlin Li, Xin Tao, Chun Yuan, and Yu-Wing Tai. Devit: Deformed vision transformers in video inpainting. In *Proceedings of the 30th ACM International Conference on Multimedia (ACMMM)*, pages 779–789, 2022. 1, 2, 3, 4
- [3] Nian Cai, Zhenghang Su, Zhineng Lin, Han Wang, Zhijing Yang, and Bingo Wing-Kuen Ling. Blind inpainting using the fully convolutional neural network. *The Visual Computer*, 33:249–261, 2017. 3
- [4] Chenjie Cao, Qiaole Dong, and Yanwei Fu. Learning prior feature and attention enhanced image inpainting. In *Proceedings of the European Conference on Computer Vision (ECCV)*, pages 306–322, 2022. 3
- [5] Ya-Liang Chang, Zhe Yu Liu, Kuan-Ying Lee, and Winston Hsu. Free-form video inpainting with 3d gated convolution and temporal patchgan. In *Proceedings of the IEEE/CVF International Conference on Computer Vision (ICCV)*, pages 9066–9075, 2019. 2, 6
- [6] Xiang Chen, Hao Li, Mingqiang Li, and Jinshan Pan. Learning a sparse transformer network for effective image deraining. In *Proceedings of the IEEE/CVF Conference on Computer Vision and Pattern Recognition (CVPR)*, pages 5896–5905, 2023. 5
- [7] Nicolas Cherel, Andrés Almansa, Yann Gousseau, and Alasdair Newson. Infusion: Internal diffusion for video inpainting. *arXiv preprint arXiv:2311.01090*, 2023. 1
- [8] Qiaole Dong, Chenjie Cao, and Yanwei Fu. Incremental transformer structure enhanced image inpainting with masking positional encoding. In *Proceedings of the IEEE/CVF Conference on Computer Vision and Pattern Recognition (CVPR)*, pages 11358–11368, 2022. 3
- [9] Chen Gao, Ayush Saraf, Jia-Bin Huang, and Johannes Kopf. Flow-edge guided video completion. In *Proceedings of the European Conference on Computer Vision (ECCV)*, pages 713–729, 2020. 2, 6
- [10] Yuchao Gu, Lijuan Wang, Ziqin Wang, Yun Liu, Ming-Ming Cheng, and Shao-Ping Lu. Pyramid constrained self-attention network for fast video salient object detection. In *Proceedings of the AAAI conference on artificial intelligence (AAAI)*, pages 10869–10876, 2020. 4
- [11] Zhang Haotian, Mai Long, Wang Hailin, JinZha ando wen, and Ning Xu; John Collomosse. An internal learning approach to video inpainting. In *Proceedings of the IEEE/CVF International Conference on Computer Vision (ICCV)*, pages 2720–2729, 2019. 7
- [12] Jiabin Huang, Sing Bing Kang, Narendra Ahuja, and Johannes Kopf. Temporally coherent completion of dynamic video. *ACM Transactions on Graphics (TOG)*, 35(6):196.1–196.11, 2016. 6
- [13] Ge-Peng Ji, Yu-Cheng Chou, Deng-Ping Fan, Geng Chen, Huazhu Fu, Debesh Jha, and Ling Shao. Progressively normalized self-attention network for video polyp segmentation. In *International Conference on Medical Image Computing and Computer-Assisted Intervention (MICCAI)*, pages 142–152. Springer, 2021. 4
- [14] Jaeyeon Kang, Seoung Wug Oh, and Seon Joo Kim. Error compensation framework for flow-guided video inpainting. In *Proceedings of the European Conference on Computer Vision (ECCV)*, pages 375–390, 2022. 2, 6
- [15] Lei Ke, Yu-Wing Tai, and Chi-Keung Tang. Occlusion-aware video object inpainting. In *Proceedings of the IEEE/CVF International Conference on Computer Vision (ICCV)*, pages 14468–14478, 2021. 2
- [16] Dahun Kim, Sanghyun Woo, Joon-Young Lee, and In So Kweon. Deep blind video decaptioning by temporal aggregation and recurrence. In *Proceedings of the IEEE/CVF Conference on Computer Vision and Pattern Recognition (CVPR)*, pages 4263–4272, 2019. 2, 6
- [17] Dahun Kim, Sanghyun Woo, Joon-Young Lee, and In So Kweon. Recurrent temporal aggregation framework for deep video inpainting. *IEEE Transactions on Pattern Analysis and Machine Intelligence (TPAMI)*, 42(5):1038–1052, 2020. 6
- [18] Wei-Sheng Lai, Jia-Bin Huang, Oliver Wang, Eli Shechtman, Ersin Yumer, and Ming-Hsuan Yang. Learning blind video temporal consistency. In *Proceedings of the European Conference on Computer Vision (ECCV)*, pages 179–195, 2018. 7
- [19] Sungho Lee, Seoung Wug Oh, DaeYeun Won, and Seon Joo Kim. Copy-and-paste networks for deep video inpainting. In *Proceedings of the IEEE/CVF International Conference on Computer Vision (ICCV)*, pages 4413–4421, 2019. 2, 6, 7
- [20] Ang Li, Shanshan Zhao, Xingjun Ma, M. Gong, Jianzhong Qi, Rui Zhang, Dacheng Tao, and R. Kotagiri. Short-term and long-term context aggregation network for video inpainting. In *Proceedings of the European Conference on Computer Vision (ECCV)*, pages 728–743, 2020. 2, 6
- [21] Chun-Yi Li, Yen-Yu Lin, and Wei-Chen Chiu. Decontamination transformer for blind image inpainting. In *ICASSP 2023-2023 IEEE International Conference on Acoustics, Speech and Signal Processing (ICASSP)*, pages 1–5. IEEE, 2023. 3
- [22] Qiufu Li, Linlin Shen, Sheng Guo, and Zhihui Lai. Wavelet integrated cnns for noise-robust image classification. In *Proceedings of the IEEE/CVF Conference on Computer Vision and Pattern Recognition (CVPR)*, pages 7243–7252, 2020. 4
- [23] Qiufu Li, Linlin Shen, Sheng Guo, and Zhihui Lai. Wavecnet: Wavelet integrated cnns to suppress aliasing effect for noise-robust image classification. *IEEE Transactions on Image Processing (TIP)*, 30:7074–7089, 2021. 4
- [24] Xiaoguang Li, Qing Guo, Di Lin, Ping Li, Wei Feng, and Song Wang. Misf: Multi-level interactive siamese filtering for high-fidelity image inpainting. In *Proceedings of the IEEE/CVF Conference on Computer Vision and Pattern Recognition (CVPR)*, pages 1869–1878, 2022. 3
- [25] Xin Li, Zhikuan Wang, Chenglizhao Chen, Chunfeng Tao, Yuanbo Qiu, Junde Liu, and Baile Sun. Semid: Blind image inpainting with semantic inconsistency detection. *Tsinghua Science and Technology*, 29(4):1053–1068, 2024. 3

- [26] Zhen Li, Cheng-Ze Lu, Jianhua Qin, Chun-Le Guo, and Ming-Ming Cheng. Towards an end-to-end framework for flow-guided video inpainting. In *Proceedings of the IEEE/CVF Conference on Computer Vision and Pattern Recognition (CVPR)*, pages 17562–17571, 2022. 2, 6, 7, 8
- [27] Qiankun Liu, Zhentao Tan, Dongdong Chen, Qi Chu, Xiyang Dai, Yinpeng Chen, Mengchen Liu, Lu Yuan, and Nenghai Yu. Reduce information loss in transformers for pluralistic image inpainting. In *Proceedings of the IEEE/CVF Conference on Computer Vision and Pattern Recognition (CVPR)*, pages 11347–11357, 2022. 3
- [28] Rui Liu, Hanming Deng, Yangyi Huang, Xiaoyu Shi, Lewei Lu, Wenxiu Sun, Xiaogang Wang, Jifeng Dai, and Hongsheng Li. Fuseformer: Fusing fine-grained information in transformers for video inpainting. In *Proceedings of the IEEE/CVF International Conference on Computer Vision (ICCV)*, pages 14040–14049, 2021. 1, 2, 3, 4, 6, 7, 8
- [29] Ruixin Liu, Bairong Li, and Yuesheng Zhu. Temporal group fusion network for deep video inpainting. *IEEE Transactions on Circuits and Systems for Video Technology (TCSVT)*, 32(6):3539–3551, 2022. 2
- [30] Yang Liu, Jinshan Pan, and Zhixun Su. Deep blind image inpainting. *arXiv preprint arXiv:1712.09078*, 2017. 3
- [31] Stephane G Mallat. A theory for multiresolution signal decomposition: the wavelet representation. *IEEE Transactions on Pattern Analysis and Machine Intelligence (TPAMI)*, 11(4):674–693, 1989. 5
- [32] F. Perazzi, J. Pont-Tuset, B. McWilliams, L. Van Gool, and A. Sorkine-Hornung. A benchmark dataset and evaluation methodology for video object segmentation. In *Proceedings of the IEEE/CVF Conference on Computer Vision and Pattern Recognition (CVPR)*, pages 724–732, 2016. 6
- [33] Shruti S Phutke, Ashutosh Kulkarni, Santosh Kumar Vipparthi, and Subrahmanyam Murala. Blind image inpainting via omni-dimensional gated attention and wavelet queries. In *Proceedings of the IEEE/CVF Conference on Computer Vision and Pattern Recognition (CVPR) Workshops*, pages 1251–1260, 2023. 7
- [34] Jingjing Ren, Qingqing Zheng, Yuanyuan Zhao, Xuemiao Xu, and Chen Li. Diformer: Discrete latent transformer for video inpainting. In *Proceedings of the IEEE/CVF Conference on Computer Vision and Pattern Recognition (CVPR)*, pages 3511–3520, 2022. 1, 2, 3, 4
- [35] Jenny Schmalzfuss, Erik Scheurer, Heng Zhao, Nikolaos Karantzas, Andrés Bruhn, and Demetrio Labate. Blind image inpainting with sparse directional filter dictionaries for lightweight cnns. *Journal of Mathematical Imaging and Vision (JMIV)*, pages 1–17, 2022. 2
- [36] Oh Seoung, Wug, Lee Sungho, Lee Joon-Young, and Kim Seon, Joo. Onion-peel networks for deep video completion. In *Proceedings of the IEEE/CVF International Conference on Computer Vision (ICCV)*, pages 4402–4411, 2019. 2, 7
- [37] Pourya Shamsolmoali, Masoumeh Zareapoor, and Eric Granger. Transinpaint: Transformer-based image inpainting with context adaptation. In *Proceedings of the IEEE/CVF International Conference on Computer Vision (ICCV)*, pages 849–858, 2023. 3
- [38] Vishnu Sanjay Ramiya Srinivasan, Rui Ma, Qiang Tang, Zili Yi, and Zhan Xu. Spatial-temporal residual aggregation for high resolution video inpainting. *arXiv preprint arXiv:2111.03574*, 2021. 2
- [39] Juan Wang, Chunfeng Yuan, Bing Li, Ying Deng, Weiming Hu, and Stephen Maybank. Self-prior guided pixel adversarial networks for blind image inpainting. *IEEE Transactions on Pattern Analysis and Machine Intelligence (TPAMI)*, 45(10):12377–12393, 2023. 2, 3
- [40] Jianan Wang, Zhiliang Wu, Hanyu Xuan, and Yan Yan. Text-video completion networks with motion compensation and attention aggregation. In *Proc. IEEE Int. Conf. Acoust. Speech Signal Process. (ICASSP)*, pages 2990–2994, 2024. 2
- [41] Yi Wang, Xin Tao, Xiaojuan Qi, Xiaoyong Shen, and Jiaya Jia. Image inpainting via generative multi-column convolutional neural networks. In *Proceedings of the Advances in neural information processing systems (NIPS)*, 2018. 2, 6
- [42] Yi Wang, Ying-Cong Chen, Xin Tao, and Jiaya Jia. Vcnet: A robust approach to blind image inpainting. In *Proceedings of the European Conference on Computer Vision (ECCV)*, pages 752–768, 2020. 2, 3
- [43] Zhiliang Wu, Kang Zhang, Hanyu Xuan, Jian Yang, and Yan Yan. Dapc-net: Deformable alignment and pyramid context completion networks for video inpainting. *IEEE Signal Processing Letters (SPL)*, 28:1145–1149, 2021. 7
- [44] Zhiliang Wu, Changchang Sun, Hanyu Xuan, and Yan Yan. Deep stereo video inpainting. In *Proc. IEEE/CVF Conf. Comput. Vis. Pattern Recognit. (CVPR)*, pages 5693–5702, 2023. 1
- [45] Zhiliang Wu, Changchang Sun, Hanyu Xuan, Kang Zhang, and Yan Yan. Divide-and-conquer completion network for video inpainting. *IEEE Transactions on Circuits and Systems for Video Technology (TCSVT)*, 33(6):2753–2766, 2023. 2, 7
- [46] Zhiliang Wu, Hanyu Xuan, Changchang Sun, Weili Guan, Kang Zhang, and Yan Yan. Semi-supervised video inpainting with cycle consistency constraints. In *Proceedings of the IEEE/CVF Conference on Computer Vision and Pattern Recognition (CVPR)*, pages 22586–22595, 2023. 1
- [47] Zhiliang Wu, Kang Zhang, Changchang Sun, Hanyu Xuan, and Yan Yan. Flow-guided deformable alignment network with self-supervision for video inpainting. In *Proc. IEEE Int. Conf. Acoust. Speech Signal Process. (ICASSP)*, pages 1–5, 2023. 2
- [48] Zhiliang Wu, Changchang Sun, Hanyu Xuan, Gaowen Liu, and Yan Yan. Waveformer: Wavelet transformer for noise-robust video inpainting. In *Proc. AAAI Conf. Artif. Intell. (AAAI)*, pages 6180–6188, 2024. 5, 6, 7, 8
- [49] Ning Xu, Linjie Yang, Yuchen Fan, Jianchao Yang, Dingcheng Yue, Yuchen Liang, Brian Price, Scott Cohen, and Thomas Huang. Youtube-vos: Sequence-to-sequence video object segmentation. In *Proceedings of the European Conference on Computer Vision (ECCV)*, pages 603–619, 2018. 6
- [50] Rui Xu, Xiaoxiao Li, Bolei Zhou, and Chen Change Loy. Deep flow-guided video inpainting. In *Proceedings of the IEEE/CVF Conference on Computer Vision and Pattern Recognition (CVPR)*, pages 3723–3732, 2019. 2, 6

- [51] Yongsheng Yu, Heng Fan, and Libo Zhang. Deficiency-aware masked transformer for video inpainting. *arXiv preprint arXiv:2307.08629*, 2023. [1](#)
- [52] Yanhong Zeng, Jianlong Fu, and Hongyang Chao. Learning joint spatial-temporal transformations for video inpainting. In *Proceedings of the European Conference on Computer Vision (ECCV)*, pages 3723–3732, 2020. [1](#), [2](#), [3](#), [4](#), [6](#), [7](#), [8](#)
- [53] Kaidong Zhang, Jingjing Fu, and Dong Liu. Inertia-guided flow completion and style fusion for video inpainting. In *Proceedings of the IEEE/CVF Conference on Computer Vision and Pattern Recognition (CVPR)*, pages 5982–5991, 2022. [2](#)
- [54] Kaidong Zhang, Jingjing Fu, and Dong Liu. Flow-guided transformer for video inpainting. In *Proceedings of the European Conference on Computer Vision (ECCV)*, pages 74–90, 2022. [1](#), [2](#), [3](#), [4](#), [6](#), [7](#), [8](#)
- [55] Richard Zhang, Phillip Isola, Alexei A Efros, Eli Shechtman, and Oliver Wang. The unreasonable effectiveness of deep features as a perceptual metric. In *Proceedings of the IEEE/CVF Conference on Computer Vision and Pattern Recognition (CVPR)*, pages 586–595, 2018. [7](#)
- [56] Yanni Zhang, Zhiliang Wu, and Yan Yan. Pfta-net: Progressive feature alignment and temporal attention fusion networks for video inpainting. In *Proc. IEEE Int. Conf. Image Process. (ICIP)*, pages 191–195, 2023. [2](#)
- [57] Haoru Zhao, Zhaorui Gu, Bing Zheng, and Haiyong Zheng. Transcnn-hae: Transformer-cnn hybrid autoencoder for blind image inpainting. In *Proceedings of the 30th ACM International Conference on Multimedia (ACMMM)*, pages 6813–6821, 2022. [3](#)
- [58] Weiyang Zheng, Cheng Xu, Xuemiao Xu, Wenxi Liu, and Shengfeng He. Ciri: Curricular inactivation for residue-aware one-shot video inpainting. In *Proceedings of the IEEE/CVF International Conference on Computer Vision (ICCV)*, pages 13012–13022, 2023. [1](#)
- [59] Shangchen Zhou, Chongyi Li, Kelvin CK Chan, and Chen Change Loy. Propainter: Improving propagation and transformer for video inpainting. In *Proceedings of the IEEE/CVF International Conference on Computer Vision (ICCV)*, pages 10477–10486, 2023. [6](#)
- [60] Shihao Zhou, Duosheng Chen, Jinshan Pan, Jinglei Shi, and Jufeng Yang. Adapt or perish: Adaptive sparse transformer with attentive feature refinement for image restoration. In *Proceedings of the IEEE/CVF Conference on Computer Vision and Pattern Recognition (CVPR)*, pages 2952–2963, 2024. [5](#)
- [61] Xueyan Zou, Linjie Yang, Ding Liu, and Yong Jae Lee. Progressive temporal feature alignment network for video inpainting. In *Proceedings of the IEEE/CVF Conference on Computer Vision and Pattern Recognition (CVPR)*, pages 16448–16457, 2021. [2](#)